Time-Resolved Solid-State NMR Spectroscopy of 5-Enolpyruvylshikimate-3-phosphate Synthase†

Richard J. Appleyard, Wendy A. Shuttleworth, and Jeremy N. S. Evans*

Department of Biochemistry and Biophysics, Washington State University, Pullman, Washington 99164-4660

Received November 29, 1993; Revised Manuscript Received March 28, 1994®

ABSTRACT: The novel technique of time-resolved solid-state NMR spectroscopy has been used to characterize the enzyme, 5-enolpyruvylshikimate-3-phosphate (EPSP) synthase, in both the forward and reverse directions over time periods ranging from 5 to 300 ms. The wealth of data currently available for EPSP synthase, in particular the pre-steady-state kinetics performed using chemical quench-flow experiments [Anderson, K. S., Sikorski, J. A., & Johnson, K. A. (1988) *Biochemistry 27*, 7395–7406], has made the enzyme an obvious choice as a proving ground for this new technique. Pre-steady-state ^{13}C TOSS CP-MAS spectra have been obtained with a much improved signal-to-noise ratio, and corrections have been made to some previously reported assignments [Evans, J. N. S., Appleyard, R. J., & Shuttleworth, W. A. (1993) *J. Am. Chem. Soc. 115*, 1588–1590]. Peak fitting has allowed the extrapolation of NMR integral intensities of species involved in the reaction. These show a good correlation with concentrations calculated by simulations using the kinetic parameters obtained from the chemical quench-flow experiments. It is proposed that careful optimization of the contact time used will be necessary to obtain accurate, relative concentrations that will enable an independent kinetic simulation by time-resolved solid-state NMR. The technique shows much promise due to its nondestructive quenching procedure, which allows the direct observation of enzyme intermediates on a reaction pathway. However, its requirement of significantly larger amounts of enzyme does limit the technique to those proteins which naturally occur in high abundance or have been hyperexpressed.

An important aspect of understanding enzymatic reaction mechanisms is the detection and structural determination of the intermediates in a reaction pathway. For this, pre-steady-state kinetics is preferred over steady-state kinetics because events on the enzyme are observed as they occur. To date, most pre-steady-state procedures require rapid sampling techniques such as UV–vis and IR spectroscopy, but these provide limited structural information. The alternative application of more powerful structural methods such as X-ray crystallography and NMR spectroscopy has been restricted because of their relatively long sampling times. Some X-ray crystal structures have been obtained on relatively short time scales, but to date the time resolution achieved has been 1–3 s with Laue diffraction methods (Hajdu et al., 1987a,b; Farber et al., 1988; Hajdu & Johnson, 1990), although in theory Laue methods can achieve time resolutions in the millisecond regime (Moffat, 1989).

Other pre-steady-state techniques use quenching reagents to halt the reaction and then study the reaction mixture at leisure by various analytical techniques, such as chromatography. The chemical quench–flow technique (Anderson et al., 1988c) has been used to identify one enzyme–intermediate complex for 5-enolpyruvylshikimate-3-phosphate (EPSP) synthase (EC 2.5.1.19), with subsequent analysis by solution-state NMR spectroscopy (Anderson et al., 1988a). EPSP synthase is a monomer with a molecular mass of 46 kDa and a key enzyme in the aromatic amino acid biosynthetic pathway that catalyzes (Scheme 1) the formation of EPSP (**4**) and P_i from shikimate 3-phosphate (S3P, **1**) and phosphoenolpyruvate (PEP, **2**) via the enzyme-bound intermediate (E·I, **3**) (Levin & Sprinson, 1964). The vulnerability of relatively unstable enzyme–intermediate complexes to a chemical quench is the major concern of this technique. It is important to realize that an intermediate that has been isolated might not be on the reaction pathway, but might have resulted from the rearrangement or breakdown of another intermediate (Fersht, 1985). It would therefore seem preferable to detect the intermediate directly *while it is still bound to the enzyme*, and a less disruptive method of quenching is required in order to do this.

The idea of thermal quenching first came to light in the 1960s. The essential requirement of any rapid quench process is that it be fast compared to the reaction being studied. A technique was devised (Bray, 1961; Ballou & Palmer, 1974) to freeze rapidly a reaction solution at a rate on the order of 10^5 K s^{-1} and then to examine the frozen sample by ESR spectroscopy. Studies (Plattner & Bachmann, 1982; Bald, 1985; Mayer, 1985) of the effects of freezing on proteins have determined that the destructive aspect of the process is the formation of hexagonal ice. So long as the freezing process is fast ($\geq 10^5$ K s^{-1}) and/or cryoprotectants (e.g., glycerol) are used, the majority of enzyme activity can be retained throughout the freezing process. We have also found that the effects of the rapid freezing technique (Evans et al., 1992; Appleyard & Evans, 1993) are consistent with minimal possible damage to the protein.

Interestingly, the coupling of the thermal quenching technique with NMR spectroscopy has not been carried out until now. This might well be attributed to the fact that until the introduction of cross-polarization (CP) and magic angle spinning (MAS), solid-state NMR did not attain the high resolution of its solution-state counterpart. But solid-state NMR has the advantage of having no known molecular mass limit, unlike the current ~50-kDa limit for the solution-state heteronuclear NMR studies of enzymes (Evans, 1992).

† This work was supported by the National Institutes of Health (GM43215), and the WSU NMR Center equipment was supported by NIH Grant RR 0631401, NSF Grant CHE-9115282, and Battelle Pacific Northwest Laboratories Contract No. 12-097718-A-L2.

* Author to whom correspondence should be addressed.

® Abstract published in *Advance ACS Abstracts,* May 15, 1994.

0006-2960/94/0433-6812$04.50/0

Scheme 1: Reaction Catalyzed by 5-Enolpyruvylshikimate-3-phosphate Synthase

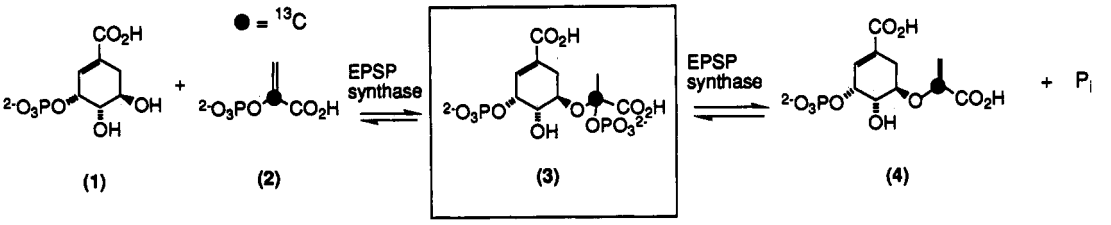

However, the amount of structural information available is limited because the internuclear interactions, e.g., dipolar coupling, are removed by MAS in order to reduce line widths to an acceptable level. Recently, a number of solid-state NMR pulse sequences have been developed (Raleigh et al., 1988; Gullion & Schaefer, 1989; Copié et al., 1990; Holl et al., 1990; Marshall et al., 1990) that can selectively reintroduce the dipolar interaction and allow the determination of very accurate distances (Christensen & Schaefer, 1993; Garbow & McWherter, 1993; Lakshmi et al., 1993). The prospect of detailed internuclear distance measurements puts solid-state NMR on the verge of a transformation similar to that which solution-state NMR underwent with the introduction of two-dimensional techniques.

Here, we report the pre-steady-state characterization of the reaction catalyzed by EPSP synthase by time-resolved solid-state NMR. The cloned *Escherichia coli* (*E. coli*) gene has been hyperexpressed (Shuttleworth et al., 1992), so that the bacterial enzyme is available in the gram quantities required for these experiments. This enzyme has been studied extensively by kinetic and physical methods (Anderson et al., 1988b,c) and is one of the few enzymes for which a full kinetic and thermodynamic profile has been determined. This laboratory was the first to make an NMR assignment for the EPSP synthase–intermediate complex (E·I, 3) (Scheme 1) under steady-state conditions (Barlow et al., 1989; Evans, 1992), which was later confirmed by another laboratory (Anderson et al., 1990). These qualities make the enzyme the perfect choice as a test system for the time-resolved solid-state NMR technique. We recently reported our preliminary studies showing the first detection of the EPSP synthase–intermediate complex by time-resolved solid-state NMR (Evans et al., 1993). The current study completes the time-resolved solid-state NMR characterization in both the forward and reverse directions. We report further improvements in the methods for carrying out this new technique and also demonstrate the feasibility of extracting pre-steady-state kinetic constants from time-resolved solid-state NMR data.

MATERIALS AND METHODS

Chemicals and Enzymes. All chemicals and enzymes, including PEP, NADH, ADP, lysozyme, deoxyribonuclease, lactate dehydrogenase, and pyruvate kinase, were purchased from Sigma (St. Louis, MO) except where stated otherwise. Potassium [2-^{13}C]PEP was purchased from MSD Isotopes (Montreal, Canada).

Growth of Cells. *E. coli* cells, BL21 (λDE3) (pLysE) (pWS230) (Shuttleworth et al., 1992), were grown in LB broth containing selection antibiotics (ampicillin, kanamycin, and chloramphenicol) for 4 h and then induced with IPTG. After an additional 4 h, the cells were harvested by centrifugation in a DuPont Sorvall RC-4B centrifuge. Cells were stored for periods of up to 2 months at −70 °C.

Enzyme Activity Assay and Protein Determination. EPSP synthase activity was routinely assayed in the reverse direction by method 1 of Lewendon and Coggins (1983). Protein was determined by the method of Bradford (1976).

Enzyme Purification. EPSP synthase was purified by a modification of established methods (Duncan et al., 1984; Padgette et al., 1987), as outlined elsewhere (Shuttleworth et al., 1992). Enzyme preparations were found to retain up to 95% of their enzymatic activity for several weeks at 4 °C and for several months if frozen rapidly in liquid nitrogen and stored at −20 °C. All enzyme manipulations other than assays were carried out at 4 °C.

Substrates. S3P was purified from cultures of *Klebsiella pneumoniae*, using an adaptation of an older method (Bondinell et al., 1971), by batch elution anion exchange chromatography on QAE Fast Flow in 300 mM ammonium bicarbonate at pH 9. Further purification was achieved by FPLC on MonoQ (Pharmacia/LKB) using a linear gradient of 10–500 mM ammonium bicarbonate at pH 9.0. S3P was located during the chromatographic steps using the thiobarbiturate assay (Millican, 1963). Once isolated, the purity was checked by ^{1}H NMR spectroscopy, and the S3P was quantitated by both thiobarbiturate and phosphate (Chen et al., 1956) assays.

[8-^{13}C]EPSP was prepared enzymatically by the overnight incubation of 200 μmol of S3P with 100 μmol of [2-^{13}C]PEP and 5 mg of EPSP synthase at room temperature. The protein was precipitated in 70% ethanol and removed by centrifugation. The reaction mixture was then eluted on MonoQ using a 10–500 mM ammonium bicarbonate gradient. Fractions containing [8-^{13}C]EPSP were located using the enzyme activity assay (*vide supra*). The [8-^{13}C]EPSP was quantitated by phosphate assay (Chen et al., 1956), and the purity was checked by ^{1}H and ^{13}C NMR spectroscopy.

ESR Spectroscopy. The ESR spectra were acquired on both Varian E9 and Bruker ESP300E spectrometers at 5 K using a liquid helium cryostat VT apparatus. Special KelF imitation rotors were made that fit into the existing 5-mm aluminum holders, so as to make the comparison between the time-resolved ESR and NMR spectroscopy experiments as easy as possible. The KelF tubes were mounted on a nylon rod so that they could be inserted into the microwave cavity.

NMR Spectroscopy. A wide-bore, 9.4-T Chemagnetics CMX-400 spectrometer, operating at 400.1 MHz for ^{1}H and 100.6 MHz for ^{13}C, was used. Zirconia rotors were used in 5- and 7-mm triple resonance, variable-temperature (VT), magic angle spinning (MAS), Chemagnetics pencil-rotor probes. The stator housing of these probes was either zirconia and/or KelF in order to maintain a low ^{13}C background. Stable spinning was achieved with a Chemagnetics spinning speed controller, which uses a microprocessor-controlled valve on the drive gas line to maintain the speed ±5 Hz. The MAS probe was of a triple gas channel (drive, bearing, and VT) design. A house compressed air line was first dried through an FTS AD-80XA air dryer and then cooled by an FTS XR-85-1 Air Jet crystal cooler. The sample temperature was controlled by a Chemagnetics VT unit and heater on the VT line, with the drive and bearing lines at approximately room temperature (~293 K). Stable VT operation has been achieved for over 7 days with this apparatus. The temperature was calibrated (Van Geet, 1970; Martin et al., 1980) using a methanol sample.

The methanol sample used to calibrate the probe is known to be insensitive to temperature gradients across the rotor due to the isotropic motion in liquids. It has been noted (Haw et al., 1986) in the literature that mismatches in the drive, bearing, and VT temperatures can lead to temperature gradients across the sample. Temperature-sensitive solid samples have been proposed (Campbell et al., 1986; Haw et al., 1986; Haw, 1988; Wehrle et al., 1990) as "NMR thermometers" due to their sensitivity to temperature gradients. However, as reported previously, (Appleyard & Evans, 1993) there have been problems with their application, and therefore neither of these samples was used. It should be noted that the probes used in these experiments are of the three gas delivery design, allowing independent cooling and spinning gases to be used. The effects of extended periods of spinning at low temperature with this apparatus were investigated (*vide infra*).

In general, the ^{13}C TOSS (total sideband suppression) CP-MAS spectra (Dixon, 1981, 1982) were acquired at 213 K using a 4-μs pulse width, a 0.5-s contact time, and a 2-s relaxation delay. An adamantane sample was used to set up the instrument (shimming, pulse width, and power determination) and reference the spectra (δ_C = 38.5, 28.5 ppm).

Sample Freezing. The slow-frozen samples were prepared *in situ*. A sample was spun slowly (<1 kHz) in the rotor at 294 K, and the system was allowed to equilibrate. The temperature was then set to 260 K, and the freezing of the sample was determined by observing the reflected RF power, which changed dramatically once the sample solidified. The process took approximately 15–60 s, depending on the size of the rotor used, giving a rate of cooling of 0.6–2.3 K s^{-1}, i.e., ~1 K s^{-1}.

The fast-frozen samples were prepared using a custom-built BioLogic MPS-51 Mixcon apparatus. The samples were loaded into the two syringes in the unit, which was equilibrated at room temperature (~294 K). The NMR rotor was contained in an aluminum receptacle filled with liquid propane and cooled in liquid nitrogen. The sample was sprayed through a 0.5-mm nozzle into the liquid propane (~85 K), which was then removed and the unit was transferred to an aluminum block (213–223 K) in a glove box under nitrogen. Any remaining liquid propane was evaporated under reduced pressure. The sample was then transferred in the aluminum receptacle (~85 K) to the spectrometer. The probe was precooled and equilibrated at 223 K. The rotor was transferred rapidly from the receptacle to the precooled stator housing, and the cooling gas was applied. The effects of exposure to room temperature during the mounting of cold samples in the probe were also investigated (*vide infra*).

Data Analysis. All computation was performed on a Silicon Graphics Incorporated (SGI) Personal Iris 4D25TG computer. NMR processing was done off-line using the FELIX (Hare Research/Biosym) software package. Peak fitting and deconvolution were performed using a subroutine within FELIX. The SGI IRIX ported version (G. Mudunuri and F. Raushel, Texas A&M University) of KINSIM (kinetic simulation program) (Barshop et al., 1983) and FITSIM (nonlinear regression control program) (Zimmerle & Frieden, 1989) were used to model the enzymatic reactions shown in this article.

RESULTS

Determination of the Freezing Time of the Freeze Quench-Flow Apparatus. Before attempting to rapidly freeze-quench enzymatic reactions, it is obviously important to characterize precisely the overall dead-time of the mixing apparatus. The dead-time is defined as the shortest quenching time possible, i.e., the time period from when mixing of the reactants occurs

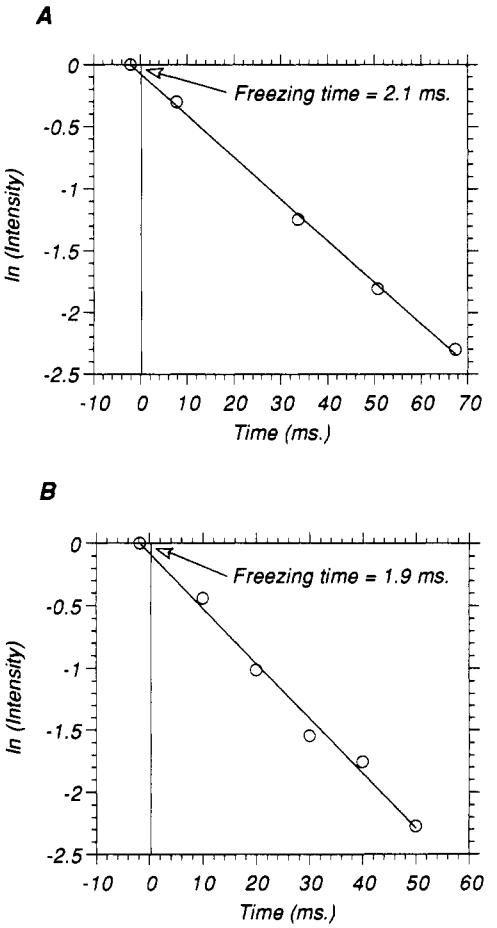

FIGURE 1: Semilog plots of the intensity of the g_6 Fe ESR signal versus the reaction time for the reaction between equine myoglobin (MbOH, 0.5 mM) and sodium azide (NaN_3, 12.5 mM) by (A) adjusting the flow rate and (B) adjusting the volume of the delay line. The spectra were acquired at 4 K on 60-μL samples at 9.406 GHz.

until when the reaction is completely stopped. For the rapid quench-flow apparatus this is made up of three distinct stages: the apparatus time (from the mixer to the nozzle), the flight time (from the nozzle to the cryogen), and the freezing time (immersion in the cryogen). The first two stages are governed by the apparatus: its maximum flow rate, the volumes of the delivery lines, the diameter of the nozzle, and the associated exit velocity. The values for these have been determined (BioLogic Instruments) as a 3-ms apparatus dead-time and a 1-ms flight time (flow rate, 7 μL ms^{-1}; nozzle diameter, 0.5 mm). With these values known, the freezing time can be determined by using a reaction with a well-characterized first-order reaction rate, e.g., equine myoglobin (MbOH) and sodium azide (NaN_3) (Goldsack et al., 1965), as described in a previous paper (Appleyard & Evans, 1993).

In brief, ESR spectroscopy was used to follow the disappearance of the high-spin (g_6) myoglobin hydrate (MbOH) by conversion to the low-spin form (MbN_3^-), which is ESR-"silent". Figure 1A,B shows two semilog plots of the intensity of the g_6 Fe signal versus the reaction time (calculated from the apparatus dead-time and the flight time). The reaction time was adjusted by altering the flow rate (Figure 1A) and the apparatus time (the volume of the delay line between the mixer and the exit nozzle) (Figure 1B). A 0.5-mm nozzle was used in both cases. The pseudo-first-order rate constants were determined from the slopes to be 2690 and 3530 s^{-1}, respectively, which was in general agreement with independent studies (Goldsack et al., 1965; Bray et al., 1973; Ballou & Palmer, 1974). The freezing time was determined by

extrapolating the plot to ln(intensity) = 0. It can be seen that this occurs 1.9–2.1 ms before the apparent zero time point. This is on the same order as previous ESR studies (Bray et al., 1973; Ballou & Palmer, 1974) and gives a rate of cooling for the rapid freezing apparatus of 1.04×10^5 K s^{-1}, i.e., $\sim 10^5$ K s^{-1}. The overall dead-time therefore is 6 ms, comprising 3 ms of apparatus, 1 ms of flight, and 2 ms of freezing time. It should be noted that all rapid mixing times shown in this article are the instrument times (apparatus and flight) only and do not include the 2-ms freezing time determined here.

Determination of Sample Transfer and Temperature Gradient Effects. Two concerns of the low-temperature NMR experiments were the exposure of the freshly prepared time point samples to room temperature when they are mounted in the solid-state NMR probe and the temperature gradients across the rotor.

The low activation energy of the $MbOH/N_3^-$ reaction (Goldsack et al., 1965) means that it is very sensitive to increased temperatures during sample transfer to the probe. Any exposure to temperatures approaching 273 K would result in the reaction proceeding and an observed decrease in the g_6 Fe signal. Two $MbOH/N_3^-$ samples were prepared in NMR rotors using the rapid freeze quench-flow apparatus, with a reaction time of 20 ms. A control sample was kept in the LN_2 ($\sim$85 K), while the other sample was mounted in the NMR probe and spun at 4 kHz for 10 min. The sample was then transferred back to the LN_2, and both samples were transferred to the KelF dummy rotors at 85 K. The KelF holders had to be used because the zirconia NMR rotors reflected microwaves and therefore would not tune in the ESR cavity. The ESR spectra of the two samples were measured at 4 K, and no significant drop in the signal intensity was observed between the samples (data not shown). This implied that there was no appreciable warming of the sample during the mounting process.

Currently it is difficult to quantify sample temperature gradients, since a methanol sample gives only an average temperature and there are not yet any applicable solid samples (refer to Materials and Methods). In order to determine the progress of the reaction during the course of the NMR acquisition, a spectrum was examined every 5 h for 20 h to check for variation in the relative signal intensities of the reaction species. In this way, we could probe for the potential thermal gradients and other sources of heat (e.g., ^1H decoupling). In two separate experiments, a 50-ms time point was generated for both the forward and reverse directions, and their ^{13}C TOSS CP-MAS spectra were obtained at –60 °C and processed every 10 000 scans (data not shown). There was no significant difference in the relative intensities for either the forward or reverse direction, although the overall intensity of the 15–20-h experiment was somewhat reduced when compared to the first 5 h. The latter effect could be attributed to a slight detuning of the probe observed over the course of the experiment, leading to an expected drop in the CP efficiency.

^{13}C TOSS CP-MAS Spectra of [2-^{13}C]PEP and [8-^{13}C]-EPSP. The [2-^{13}C]PEP (40 mM final) sample was generated using the rapid freezing apparatus by mixing with S3P (40 mM final) at a reaction time of 30 ms. The ^{13}C NMR spectrum (Figure 2A) shows a resonance at δ_C = 149.5 ppm (LW = 158 Hz) after 12 000 scans. The [8-^{13}C]EPSP sample (16 mM final) was slow-frozen *in situ*, and the ^{13}C NMR spectrum (Figure 2B) shows a resonance at δ_C = 153.1 ppm (LW = 108 Hz) after 20 000 scans. Both spectra were processed with 100-Hz line broadening.

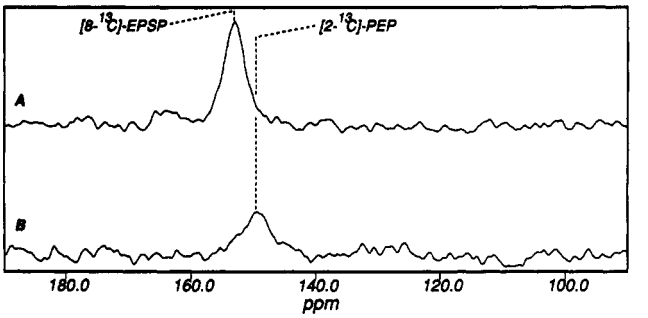

FIGURE 2: ^{13}C TOSS CP-MAS spectra of frozen solutions of (A) [2-^{13}C]PEP (rapidly frozen with 40 mM S3P) and (B) [8-^{13}C]EPSP (slow-frozen, 16 mM). The spectra were acquired on the 5-mm probe in (A) 17 000 scans and (B) 20 000 scans using a 4-μs pulse width, 0.5-s contact time, and 2-s relaxation delay and were processed with 100-Hz line broadening.

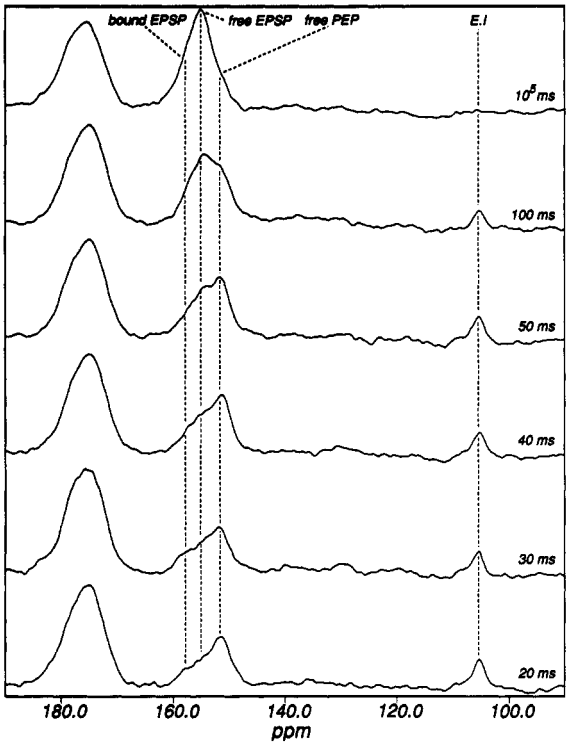

FIGURE 3: ^{13}C TOSS CP-MAS spectra of E(4 mM)·S3P(40 mM)·[2-^{13}C]PEP(40 mM) frozen mixtures, rapidly quenched in the forward direction at 20, 30, 40, 50, and 100 ms and slow-frozen after several minutes (10^5 ms). The spectra were acquired on the 7-mm probe in 12 000 scans using a 4-μs pulse width, 0.5-s contact time, and 2-s relaxation delay and were processed with 100-Hz line broadening. The spectra are shown with absolute intensity and are normalized to the protein resonance at δ_C = 174.2 ppm.

Single Turnover in the Forward Direction. The rapid freeze quench-flow apparatus was used to generate samples of EPSP synthase at different reaction times. In order to achieve the best signal-to-noise ratio, the protein was concentrated as much as possible, and the maximum concentration attainable (before causing precipitation) was $\sim$7.3 mM. By adding an appropriate volume of 200 mM S3P, the enzyme was then incubated in 10 times excess (saturating) concentration at 4 °C. The E·S3P (5.3 mM·53 mM) mixture was then loaded into one syringe, and a solution of 160 mM [2-^{13}C]PEP was loaded into the other syringe. The two syringes were then fired in a 1:4 flow rate ratio to give a final predetermined flow rate that controlled the reaction time. By adjusting the final flow rate and the delay line volume, reaction times of 5, 10, 20, 30, 40, 50, and 100 ms were obtained. The ^{13}C TOSS CP-MAS spectra of the final frozen mixtures (4 mM EPSP synthase and 40 mM S3P and [2-^{13}C]PEP) are shown in Figure

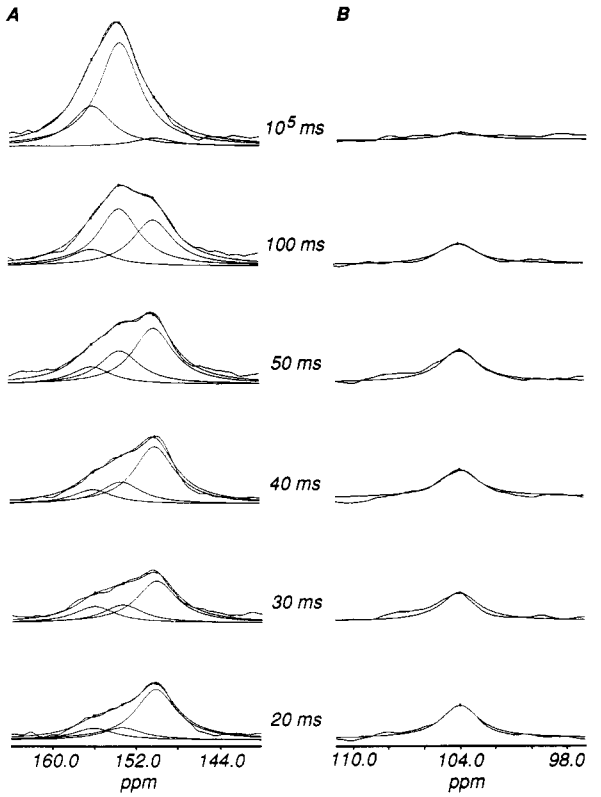

FIGURE 4: Peak-fitting of the forward reaction of EPSP synthase for (A) the enzyme-free [2-^{13}C]PEP and [8-^{13}C]EPSP and (B) the enzyme-bound intermediate (E·I). The fits were performed within FELIX using the simulated annealing algorithm.

3. For comparison, the spectrum of an equilibrated mixture (warmed to room temperature for several minutes (10^5 ms) and then refrozen) was also obtained.

The resonance due to C8 of the enzyme-bound intermediate (E·I, **3**) (Scheme 1) can be seen clearly at δ_C = 104.0 ppm, which correlates very well with the initial assignment of 104 ppm (Evans et al., 1993). The E·I signal has maximal intensity of ≤20 ms and is not present in the sample that was allowed to equilibrate at room temperature before being frozen. Several other overlapping resonances can be seen around δ_C ≈ 150 ppm. From the individual substrate and product spectra (Figure 2) and the solution state (Barlow et al., 1989), we can infer that these are the enzyme-free [2-^{13}C]PEP and [8-^{13}C]-EPSP and enzyme-bound [8-^{13}C]EPSP. Although the E·I signal could be followed by direct integration, the enzyme-free [2-^{13}C]PEP and [8-^{13}C]EPSP and enzyme-bound [8-^{13}C]-EPSP could not. These three signals were therefore resolved by deconvoluting the overlapped resonances using peak-fitting with fixed line widths. The chemical shifts used for the enzyme-free [2-^{13}C]PEP (δ_C = 150.1 ppm) and [8-^{13}C]EPSP (δ_C = 153.4 ppm) were obtained from individual ^{13}C spectra (Figure 2), and those used for the enzyme-bound [8-^{13}C]EPSP (δ_C = 156.5 ppm) were obtained from a steady-state frozen solution ^{13}C spectrum. An average LW = 130 Hz was used for all of the overlapping peaks. The E·I resonance was also integrated by the same method using δ_C = 104.0 ppm and LW = 70 Hz. The peak-fitting routine determined the peak height and integral (assuming Lorentzian line shape) for each time point, and the fitted spectra are shown in Figure 4. The peak intensities of all of the individual species were normalized to the protein carbonyl resonance at δ_C = 174.2 ppm, in order to account for experimental variations in the sample volume due to different mixing programs and delay lines.

The first stage of fitting the NMR integral data was to convert the arbitrary integral values into usable concentrations.

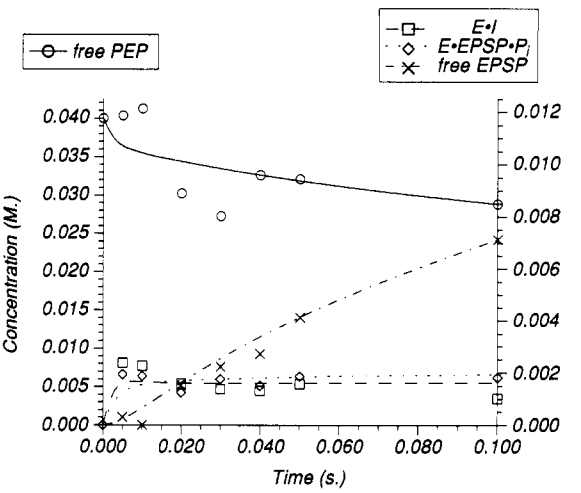

FIGURE 5: Plot of the experimental (symbols) and simulated (lines) concentrations of enzyme-free [2-^{13}C]PEP and [8-^{13}C]EPSP and enzyme-bound E·I and [8-^{13}C]EPSP against the reaction time in the forward direction. Simulations were performed using the sequential ordered mechanism, a full set of rate constants (Anderson et al., 1988c), and starting concentrations of 4 mM E·S3P, 36 mM S3P, and 40 mM [2-^{13}C]PEP. The experimental concentrations were calculated using conversion factors for each species determined from the simulation.

In our case, the integral–concentration relationship can be determined from the NMR spectra of the free substrates and products or an equilibrated enzyme solution by using the overall K_{eq} = 180. In the forward direction, the integrals were standardized against the EPSP signal at equilibrium (Figure 3, 10^5 ms) and alone in frozen solution (Figure 2B). A kinetic simulation was performed using the equilibrium-ordered mechanism (Scheme 2) and the starting concentrations of 4 mM E·S3P, 36 mM S3P, and 40 mM [2-^{13}C]PEP. The previously determined kinetic rate constants (Anderson et al., 1988c) were used as a starting set, but the kinetic parameters could not be fit to these converted concentrations either by manual interaction or with a computer fitting program (FITSIM). The nonconvergent fit was attributed to incorrect relative intensities from the NMR integrals (see Discussion); however, there was still a good correlation between each set of experimental intensities and the corresponding simulated concentrations. By calculating early (10 ms) and final equilibrium concentrations for each species using a simulation with the previously determined kinetic rate constants, the integrals for each species were standardized independently. The resultant concentrations are plotted along with the simulated data in Figure 5.

Single Turnover in the Reverse Direction. The characterization of EPSP synthase by time-resolved solid-state NMR was also performed in the reverse direction. The same enzyme concentrations were used, but instead the appropriate volume of 200 mM P_i was added to incubate the protein in 10 times excess concentration at 4 °C. The E·P_i (5.3 mM·53 mM) mixture and the 160 mM [8-^{13}C]EPSP were used in the rapid freeze quench-flow apparatus, and samples (4 mM EPSP synthase and 40 mM S3P and [8-^{13}C]EPSP) reacted at 10, 50, and 100 ms and fully equilibrated (10^5 ms) were obtained. The ^{13}C TOSS CP-MAS spectra were acquired and are shown in Figure 6. The resonance due to E·I is seen again at δ_C = 104.0 ppm and has maximal intensity between 50 and 100 ms. Several overlapping resonances are seen again around δ_C ≈ 150 ppm, but the major peak observed at δ_C = 153.4 ppm is clearly due to enzyme-free [8-^{13}C]EPSP. There is a clear majority of [8-^{13}C]EPSP throughout the time course and even in the fully equilibrated spectrum (Figure 6, 10^5 ms). This

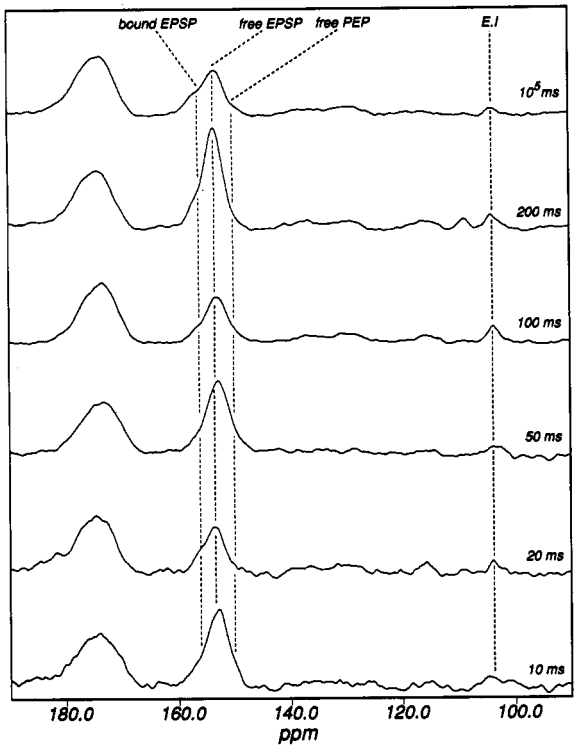

FIGURE 6: ^{13}C TOSS CP-MAS spectra of E(4 mM)·S3P(40 mM)·[2-^{13}C]PEP(40 mM) frozen mixtures, rapidly quenched at 10, 20, 50, 100, and 200 ms and slow-frozen after several minutes (10^5 ms). The spectra were acquired on the 5-mm probe in 60 000 scans using a 4-μs pulse width, 0.5-s contact time, and 2-s relaxation delay and were processed with 100-Hz line broadening. The spectra are shown with absolute intensity and are normalized to the protein resonance at δ_C = 174.2 ppm.

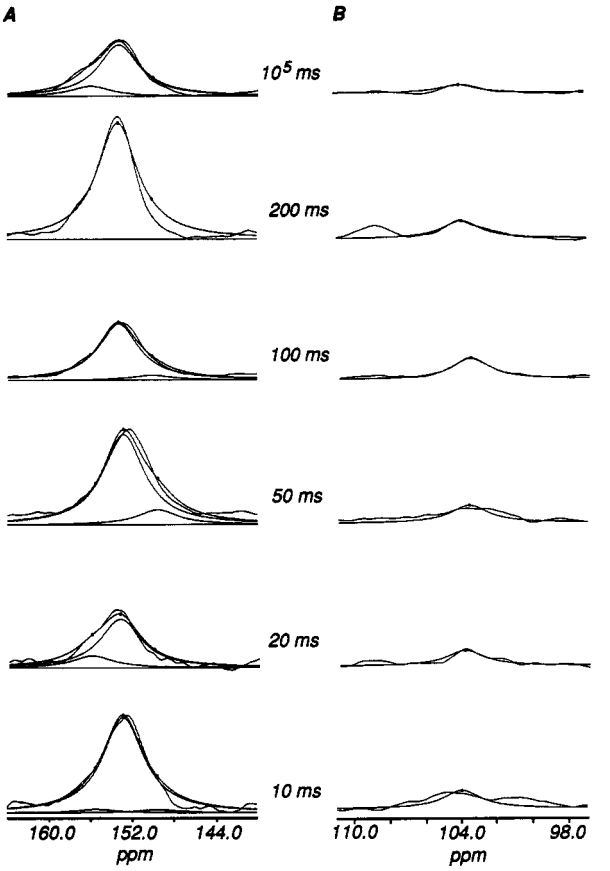

FIGURE 7: Peak-fitting of the reverse reaction of EPSP synthase for (A) the enzyme-free [8-^{13}C]EPSP and (B) the enzyme-bound intermediate (E·I). The fits were performed within FELIX using the simulated annealing algorithm.

is not unexpected since K_{eq} gives a final concentration of [8-^{13}C]-EPSP = 37.2 mM.

Peak-fitting was used again to resolve and integrate the reaction species in the spectra. The chemical shifts and line widths used were the same as those used for the forward direction, and the deconvoluted spectra are shown in Figure 7. The peak intensities of all the individual species were normalized to the protein carbonyl resonance at δ_C = 174.2 ppm.

A kinetic simulation was performed again using the equilibrium-ordered mechanism (Scheme 2), the starting concentrations of 4 mM E, 40 mM P_i, and 40 mM [8-^{13}C]-EPSP, and the previously determined kinetic rate constants (Anderson et al., 1988c). Again, the kinetic parameters could not be fit to the converted concentrations either manually or by program, but there was a reasonable correlation between the experimental and the corresponding simulation data. The experimental integrals were standardized using concentrations calculated for each species by simulation as before. The resultant concentrations are plotted along with the simulated data in Figure 8.

DISCUSSION

Assignment of the EPSP Synthase Reaction Species in the Solid State. The chemical shift of δ_C = 104.0 ppm for the E·I complex in the solid state is different from the δ_C = 107.2 ppm previously observed in the solution state (Barlow et al., 1989). This shift can be attributed to the slight changes in the environment on going from the solution to the frozen state. The different referencing used for the solution (dioxane/D_2O, δ_C = 67.4 ppm) and the solid (adamantane, δ_C(quaternary) = 38.5 ppm) was found to be internally consistent; e.g., using adamantane referencing, δ_C(dioxane) = 67.3 ppm.

At the high concentrations used in previous NMR experiments, EPSP synthase is known to undergo an unusual side reaction, forming the EPSP ketal (Barlow et al., 1989; Anderson et al., 1990; Leo et al., 1990). Since the ketal has a very similar C8 chemical shift, it is possible that it would interfere with the assignment of the enzyme–intermediate. However, this can be discounted immediately since its rate of formation (0.000 033 s^{-1}) is approximately a millionfold slower than the turnover rate of the enzyme intermediate (1200 s^{-1}) (Anderson et al., 1988c). In addition, we have observed formation of the EPSP ketal only under steady-state conditions in excess phosphate buffer over a period of 48 h. Since the system clearly is not at equilibrium during a single turnover, it is implausible for the ketal to interfere with the assignment, and the resonance at 104.0 ppm can only be assigned to the enzyme–intermediate.

Originally, we assigned (Evans et al., 1993) the resonances at δ_C = 151 and 155 ppm to enzyme-bound PEP and EPSP. The relatively poor signal-to-noise ratios and large spinning sidebands (associated with the protein carbonyl resonances) made accurate chemical shift assignment very difficult in our initial spectra. We also had been unable to obtain spectra for the frozen solutions of [2-^{13}C]PEP and [8-^{13}C]EPSP alone, which we attributed to possible motion of the free substrates and products in the frozen solution. By using the TOSS pulse sequence (Dixon, 1981, 1982) and longer acquisitions, we obtained ^{13}C spectra of [2-^{13}C]PEP and [8-^{13}C]EPSP alone and assigned their chemical shifts in the frozen solid state (Figure 2). A simple correlation ($\Delta\delta \approx 2.8$ ppm) was possible by comparing the solution- and solid-state chemical shifts of these and the E·I resonances. A significant improvement in the signal-to-noise ratios of the protein-containing spectra

Scheme 2: Equilibrium-Ordered Mechanism for EPSP Synthase (Anderson et al., 1988c)

$$E \underset{k_{-1}}{\overset{k_1[S3P]}{\rightleftharpoons}} E{\cdot}S3P \underset{k_{-2}}{\overset{k_2[PEP]}{\rightleftharpoons}} E{\cdot}S3P{\cdot}PEP \underset{k_{-3}}{\overset{k_3}{\rightleftharpoons}} E{\cdot}I \underset{k_{-4}}{\overset{k_4}{\rightleftharpoons}} E{\cdot}EPSP{\cdot}P_i \underset{k_{-5}[P_i]}{\overset{k_5}{\rightleftharpoons}} E{\cdot}EPSP \underset{k_{-6}[EPSP]}{\overset{k_6}{\rightleftharpoons}} E$$

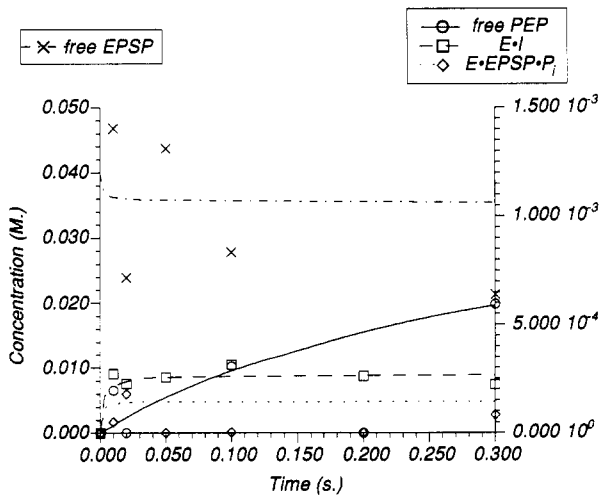

FIGURE 8: Plot of the experimental (symbols) and simulated (lines) concentrations of enzyme-free [8-^{13}C]EPSP and enzyme-bound intermediate (E•I) against the reaction time in the reverse direction. Simulations were performed using the sequential ordered mechanism, a full set of rate constants (Anderson et al., 1988c), and starting concentrations of 4 mM E, 40 mM P_i, and 40 mM [8-^{13}C]EPSP. The experimental concentrations were calculated using conversion factors for each species determined from the simulation.

was also achieved with TOSS by elimination of the large sidebands. This made deconvolution of overlapping resonances far easier and allowed a more accurate determination of integral intensities.

Having determined that it is the enzyme-free [2-^{13}C]PEP and [8-^{13}C]EPSP that are observed at δ_C = 150.1 and 153.4 ppm, respectively, we were able to assign the enzyme-bound [8-^{13}C]EPSP at δ_C = 156.5 ppm by running a steady-state experiment at the same concentrations that were used in the pre-steady state. The bound EPSP was clearly observed in the ^{13}C spectra for both the solution and frozen solid states (data not shown). However, we did not observe the ternary E•S3P•PEP complex (enzyme-bound PEP) in the forward direction since its rate of decay (k_3 = 1200 s^{-1}) is much greater than its rate of formation (k_2 = 15 μM^{-1} s^{-1}) (Anderson et al., 1988c), and it therefore never reached a detectable concentration. The complex was not observed in the reverse direction either for the same reasons (k_{-2} = 280 s^{-1} > k_{-3} = 100 s^{-1}).

Kinetic Analysis. Complete kinetic and thermodynamic analyses have only been determined for a small number of enzymes (Albery & Knowles, 1976; Fierke et al., 1987; Zimmerle et al., 1987; Sekhar & Plapp, 1990). The use of rapid chemical quench–flow studies allowed (Anderson et al., 1988c) the definition of a set of kinetic rate constants for EPSP synthase using kinetic simulation software (Barshop et al., 1983). The equilibrium-ordered mechanism that was chosen involved ordered binding of S3P followed by PEP and ordered release of P_i followed by EPSP (Scheme 1). The evidence for this came from ligand trapping experiments, which showed that S3P binding occurs with a dissociation constant close to the K_m of the enzyme, and there was a considerable lag in intermediate formation for preformed E•PEP. The converse trapping experiment for E•P_i was not possible, but the authors inferred the order of binding on the basis of the E•EPSP trapping experiments, which showed that EPSP bound rapidly to the enzyme, and the fact that high phosphate concentrations could lock EPSP onto the enzyme. In the subsequent kinetic simulation, a successful fit depended upon the constraints that the authors were able to place on the system. Using the binding and Michaelis constants for the substrates and products that had been determined separately, only 6 unknown rate constants were left out of a total of 12 rate constants defined by the equilibrium-ordered mechanism. These were also constrained by the internal equilibrium and overall equilibrium constants. The unknown rate constants were determined by best fit to the single turnover experiments (in particular) in the forward and reverse directions using trial and error adjustments within the KINSIM program. The authors presented what *prima facie* appeared to be a nice corroboration of their results by fitting all their figures from the kinetic data using the equilibrium-ordered mechanism and their final set of kinetic rate constants. They subsequently concluded (Anderson & Johnson, 1990) that their complete kinetic and thermodynamic analysis provided rigorous proof for the mechanism.

However, more recent steady-state kinetic data have shown that EPSP synthase randomly binds the substrates. Studies (Ream et al., 1992) using isothermal titration calorimetry determined that PEP formed a reasonably tight EPSP synthase binary complex with a K_d = 0.39 mM, which was only approximately 20-fold less than the K_m observed in the presence of S3P. Subsequent initial velocity studies (Gruys et al., 1992) with S3P and PEP were consistent with a sequential mechanism, but were also consistent with competitive substrate inhibition by PEP and not dead-end complex formation. The K_d for the EPSP synthase•PEP binary complex determined by this method was within a factor of 2 of the previous measurement (0.20 mM). Studies with 5-deoxy-S3P and PEP showed a mixed inhibition pattern versus PEP and not competition, which was further evidence against an equilibrium-ordered process, and studies (Gruys et al., 1993) in the reverse direction with EPSP and P_i were also inconsistent with an equilibrium-ordered mechanism. The authors therefore proposed a random-ordered mechanism (Scheme 3) to account for the new steady-state data.

As noted for the chemical quench analysis (Anderson et al., 1988c), the availability of software for the simulation of enzyme kinetics has revolutionized the fitting of pre-steady-state kinetic data, since all of the data can be fit to one mechanism and a single set of microscopic rate constants. However, it is important to be wary of validating particular mechanisms by this technique (Frieden, 1993), since a good fit of experimental data to a proposed model using a kinetic simulation program, even over a wide range of experimental conditions, does not prove a mechanism to be correct. Therefore, the claim of proof of the equilibrium-ordered mechanism (Anderson et al., 1988c; Anderson & Johnson, 1990) came from insufficient consideration for the practical limitations of the rapid chemical quench–flow data and the kinetic simulation technique. Since the K_d of the EPSP synthase•PEP binary complex is 0.39 mM, an insufficient amount (<6%) is present under the chemical quench conditions to affect the trapping experiments, and phosphate binding is even weaker, thus preventing the trapping experiments from being performed.

Scheme 3: Random-Ordered Mechanism for EPSP Synthase (Gruys et al., 1993)

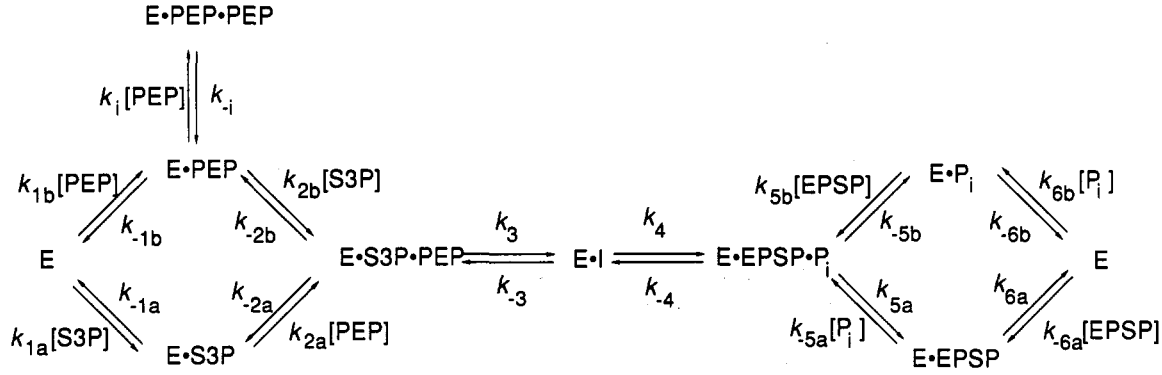

Although the random-ordered mechanism is now the generally accepted mechanism for EPSP synthase, the amount of kinetic data for this model is still limited. The steady-state analyses were important in showing inconsistencies in the assignment of the equilibrium-ordered mechanism and in providing evidence for a random-ordered mechanism. However, these experiments were only able to measure the kinetic equilibrium constants for each proposed step of the mechanism and did not provide absolute values of the k_{on}/k_{off} rates for PEP or P_i with free enzyme. This means that if we assume that the k_{off} rates for S3P and EPSP from their binary complexes and the k_{on} rates for PEP and P_i previously calculated are still correct, there are still 14 unknown rate constants out of a total of 22 for the random-ordered mechanism. There are six equilibrium constant constraints for these unknowns, but without additional k_{on}/k_{off} rates it is unlikely that a fit would converge using either the chemical quench or freeze-quench data. Since our data set is smaller than that obtained by chemical quench, any set of rate constants obtained with such a large number of unknowns would not validate the mechanism with any certainty. Therefore, fitting to this mechanism would not provide a satisfactory test of our approach.

In order to compare the freeze quench-flow and chemical quench-flow techniques, we took our freeze-quench integral data and simulations using the chemical quench rate constants and the equilibrium-ordered mechanism. The use of this mechanism is not entirely unreasonable, and it was noted (Gruys et al., 1992) that the results can be easily integrated into a random model by considering that the rate constants are simply those for the bottom half of the pathway shown in Scheme 3. If the exchange rates for the alternative binding pathways in the random model are low enough, then the equilibrium-ordered mechanism is a good first approximation.

Although in the forward direction the enzyme was preincubated with S3P, which is consistent with the equilibrium-ordered mechanism, in the reverse direction the enzyme was first mixed with P_i, which is not consistent with this mechanism. However, the enzyme was not preincubated with EPSP for several good reasons. Firstly, the hydrolase activity of EPSP synthase (Anderson et al., 1990; Leo et al., 1990) could turn over EPSP prior to the freeze-quench experiment. This was also a concern in the chemical quench experiments (Anderson et al., 1988c), which used much lower concentrations of enzyme and EPSP, and the experiments had to be completed quickly (<24 min) and the data corrected for the slow rate of hydrolysis. Secondly, there was concern that any low-level P_i contamination in the enzyme preparation could cause a premature start of the reaction when mixed with EPSP. Preincubation of the enzyme with P_i avoids these problems, and the high concentrations of EPSP and P_i (40 mM) used also avoid any lag in the reaction.

As noted in the Results section, we were unable to directly simulate the experimentally determined concentrations since the NMR integrals gave incorrect relative ratios for the reaction species. However, since there was a good visual correlation of the integral intensity data in both the forward and reverse directions, the integrals for each reaction species were standardized using concentrations determined by an independent simulation using the previously determined rate constants (Anderson et al., 1988c) and the equilibrium-ordered mechanism. The only conclusion that we may draw from this comparison is that the relative changes of each reaction species, as followed by solid-state NMR, correlate very well with those predicted. This is encouraging, since it demonstrates the feasibility of determining kinetic data using time-resolved solid-state NMR.

The scatter in the reverse data was noticeably poorer than that in the forward data. Firstly, there were difficulties with the quantitation of the enzymatically prepared [8-^{13}C]EPSP. One batch of PEP used for the standardization was found to have some free phosphate contamination, leading to a slight underestimate of the concentration. This would account for the larger variation in the intensities for EPSP between time points in the reverse direction. Secondly, the equilibrium constant is heavily in favor of products (K_{eq} = 180), and therefore the free PEP, E•I, and bound EPSP are at, or below, the detection threshold.

Chemical Quench versus Freeze-Quench. Currently, unlike the chemical quench technique, the use of the freeze-quench to determine microscopic rate constants is still under development. As mentioned above, the main problem in trying to obtain kinetic information in these experiments is that the integrals cannot be correctly correlated to the concentrations for use in a simulation. The quantifiability of ^{13}C CP-MAS NMR spectra has been addressed previously (Voelkel, 1988), and it is known that signal intensities are dependent on the kinetics of magnetization transfer during cross-polarization. The ^{13}C signal intensity is dependent on two competing factors: the ^{1}H–^{13}C magnetization transfer under the Hartmann–Hahn condition and the ^{1}H relaxation delay under spin-lock ($T_{1\rho}^H$). The former is more important at short contact times and is dependent on the type of carbon atom, while the latter is important at longer contact times and is not atom-dependent. At sufficiently long contact times, spectra are approximately quantitative, even without normalization. However, at short contact times the intensity can vary most significantly for different types of carbon, and this results in unreliable integrals and incorrect, relative quantitation of the reaction species. The latter scenario applies here, since a relatively short contact time (0.5 ms) is required due to the short $T_{1\rho}^H$ observed in frozen solutions (Appleyard & Evans, 1993). Further careful optimization of the contact time will be required to minimize this problem. However, once a

consistent relationship between integral and concentration can be determined for the frozen solution state, direct kinetic analysis using solid-state NMR data should be feasible.

A major drawback of a chemical quench-flow study is that it disrupts the enzyme structure in order to halt the reaction. In the study of EPSP synthase (Anderson et al., 1988b), a rapid, acidic chemical quench was used on the enzyme, and the reaction mixture was then analyzed by HPLC. No actual intermediate was isolated, but the formation of pyruvate was observed, and it was proposed that this was formed by breakdown of the real intermediate. It was not until a later study (Anderson et al., 1988a) that the tetrahedral intermediate (**3**, Scheme 1) was isolated free of the enzyme using a basic chemical quench and its structure characterized by solution-state NMR. This illustrates the uncertainty in assigning species isolated after a chemical quench and in whether they represent true intermediates. The authors concluded that these studies provided definitive identification of the true intermediate. While there is no doubt that this methodology did eventually allow the determination of the structure of the intermediate, the chemical quench does not allow the direct detection of an enzyme-bound intermediate.

It has been noted that NMR spectroscopy and the rapid quench technique provide a perfect complement to one another (Anderson & Johnson, 1990), and their coupling together in time-resolved solid-state NMR provides an elegant solution to the aforementioned problem by detecting the intact E·I complex. However, it is still possible that the freeze-quench process also affects protein structure, since the shearing forces of the advancing crystalline ice fronts can tear macromolecules (cell walls, membranes, and proteins) apart when a solution is frozen. In order to avoid ice crystallization, the solvent mobility must be decreased until it outweighs the thermodynamic driving force. Traditionally, protein solutions have included a cryoprotectant, e.g., glycerol, which increases the viscosity and lowers the thermodynamics. However, rapid freezing achieves the same effect by not allowing enough time for the ice front to form. Studies on the relaxation properties of glycine in rapidly frozen solution (Appleyard & Evans, 1993) have shown a highly dispersed solute, which is consistent with this hypothesis. There are also studies (Angell & Choi, 1986) suggesting that at high concentrations most solutes interfere with ice formation, and therefore the protein probably acts as its own cryoprotectant at the concentrations used in these experiments. This is confirmed by studies in this laboratory (data not shown) where the enzyme activity has been monitored throughout the rapid freezing process. At high concentrations the integrity of the protein was maintained, whereas at low concentrations activity was lost.

Another effect of the chemical quench is that substrate or product complexes with the enzyme cannot be resolved from the free substrates or products, since after the quench it is impossible to distinguish between them. The time-resolved solid-state NMR technique is able to detect bound species so long as k_{on}/k_{off} rates allow them to build up to a detectable concentration. In the case of EPSP synthase, we were able to detect the ternary complex with EPSP and P_i due to the relatively slow off-rates; however, we could not detect the ternary complex between S3P and PEP probably due to its high turnover rate (*vide supra*). The time-resolved NMR technique can run into resolution problems as well, if the bound and free species are not sufficiently separated in chemical shift. The EPSP synthase reaction is well-suited for study using ^{13}C NMR, since the vinylic carbons of the PEP substrate undergo a change in hybridization ($sp^2 \rightarrow sp^3 \rightarrow sp^2$) on formation of the intermediate complex. This results in a large shift in the observed chemical shift at C2-PEP/C8-E·I/C8-EPSP (δ_C = 150.1/104.0/153.4 ppm). However, the free substrate (PEP) and free product (EPSP) were close enough in chemical shift to overlap, along with the bound product (δ_C = 156.5 ppm). Fortunately, the chemical shifts and line widths involved were obtainable for all three resonances, and they were resolved using a peak-fitting routine. However, this may not always be possible in the case of several superimposed resonances, and then time-resolved solid-state NMR may not be applicable. Given this possibility, alternatives, such as switching to a different nucleus (e.g., ^{15}N or ^{31}P) that could be more sensitive to a change in structure during the reaction, should always be explored.

Both chemical quench-flow and freeze quench-flow techniques rely on an enzyme mechanism involving relatively slow steps in the formation or release of products, if the enzyme–intermediate is to build up to a detectable concentration. Obviously, this is a caveat of any rapid-quench technique, in that the ability to see a particular reaction species of a given mechanism will obviously depend on the relative rates of their interconversions. The inability to detect a possible intermediate does not mean that it is not involved. The intermediate could be so highly reactive in both the forward and reverse directions that it never accumulates. Since NMR spectroscopy is an inherently insensitive technique, compounded in the solid state by larger line widths, time-resolved solid-state NMR has relatively low sensitivity and resolution. This forces the requirement of large amounts of protein and excess substrates, so that the detection of an intermediate may be made possible. Since the HPLC technique is more sensitive, the chemical quench technique has better detection capabilities, and kinetic data can be obtained on a smaller sample of protein. However, solution-state NMR spectroscopy may still be required in order to positively identify a reaction species, and then large-scale chemical quenches are also required.

In addition to rapid chemical quench–flow techniques and time-resolved solid-state NMR, it is worth mentioning that Laue X-ray diffraction has also allowed the determination of structures on the pre-steady-state time scale. Crystal structures of an enzyme and pseudosubstrates have been solved on the time scale of seconds, showing a reaction in progress (Hajdu et al., 1987a,b; Farber et al., 1988; Hajdu & Johnson, 1990). Although very exciting, this technique has significant drawbacks of its own. Large *B* factors are observed for mobile atoms, which leads to a blurred image of critical regions, e.g., substrates and active-site residues. Furthermore, even in light-activated reactions, the maintenance of kinetic synchronicity of the ensemble of molecules is virtually impossible over the course of the reaction, leading to a superposition of all kinetic states in the electron density map. Therefore, while the protein structure can be determined as a function of time, the structural relationship of the substrates, intermediates, and products in the active site cannot be determined with any certainty.

CONCLUSIONS

Time-resolved solid-state NMR represents a marked step forward in the methodology for the pre-steady-state study of reactions. The far less destructive rapid freezing method is preferable over a chemical quench since it maintains the integrity of the enzyme. In this way, intermediates may be observed at the active site as the reaction progresses. The expanding number of new solid-state NMR pulse sequences to measure internuclear distances will allow the dynamic mapping of an enzyme active site. The coupling of these solid-state NMR methods with our time-resolved technique will allow the determination of individual distances at the active

site with the accuracy of X-ray crystallography, but on the millisecond time scale of traditional chemical quench–flow studies. Experiments are already under way in this laboratory to couple time-resolved solid-state NMR with REDOR NMR techniques (Holl et al., 1990; Marshall et al., 1990) in order to determine the structure of the enzyme–intermediate active-site complex. It should then be a relatively simple matter to extend this to determine key internuclear distances in enzyme–intermediate and enzyme–product complexes at different time points along the reaction pathway.

REFERENCES

Albery, W. J., & Knowles, J. R. (1976) *Biochemistry 15*, 5627–5631.

Anderson, K. S., & Johnson, K. A. (1990) *Chem. Rev. 90*, 1131–1149.

Anderson, K. S., Sikorski, J. A., Benesi, A. J., & Johnson, K. A. (1988a) *J. Am. Chem. Soc. 110*, 6577–6579.

Anderson, K. S., Sikorski, J. A., & Johnson, K. A. (1988b) *Biochemistry 27*, 1604–1610.

Anderson, K. S., Sikorski, J. A., & Johnson, K. A. (1988c) *Biochemistry 27*, 7395–7406.

Anderson, K. S., Sammons, D. R., Leo, G. C., Sikorski, J. A., Benesi, A. J., & Johnson, K. A. (1990) *Biochemistry 29*, 1460–1465.

Angell, C. A., & Choi, Y. (1986) *J. Microsc. 141*, 251–261.

Appleyard, R. J., & Evans, J. N. S. (1993) *J. Magn. Reson., Ser. B 102*, 245–252.

Bald, W. B. (1985) *J. Microsc. 140*, 17–40.

Ballou, D. P., & Palmer, G. A. (1974) *Anal. Chem. 46*, 1248–1253.

Barlow, P. N., Appleyard, R. J., Wilson, B. J. O., & Evans, J. N. S. (1989) *Biochemistry 28*, 7983–7991, 10093.

Barshop, B. A., Wrenn, R. F., & Frieden, C. (1983) *Anal. Biochem. 130*, 134–145.

Bondinell, W. E., Vnek, J., Knowles, P. F., Sprecher, M., & Sprinson, D. B. (1971) *J. Biol. Chem. 246*, 6191–6196.

Bradford, M. A. (1976) *Anal. Biochem. 72*, 248–254.

Bray, R. C. (1961) *Biochem. J. 81*, 189–193.

Bray, R. C., Lowe, D. J., Capeillere-Blandin, C., & Fielden, E. M. (1973) *Biochem. Soc. Trans. 1*, 1067–1072.

Campbell, G. C., Crosby, R. C., & Haw, J. F. (1986) *J. Magn. Reson. 69*, 191–195.

Chen, P. S., Toribara, T. Y., & Warner, H. (1956) *Anal. Chem. 28*, 1756–1758.

Christensen, A. M., & Schaefer, J. (1993) *Biochemistry 32*, 2868–2873.

Copié, V., Kolbert, A. C., Drewry, D. H., Bartlett, P. A., Oas, T. G., & Griffin, R. G. (1990) *Biochemistry 29*, 9176–9184.

Dixon, W. T. (1981) *J. Magn. Reson. 44*, 220–223.

Dixon, W. T. (1982) *J. Chem. Phys. 77*, 1800–1809.

Duncan, K., Lewendon, A., & Coggins, J. R. (1984) *FEBS Lett. 165*, 121–127.

Evans, J. N. S. (1992) in *Pulsed Magnetic Resonance: NMR, ESR and Optics (A Recognition of E. L. Hahn)* (Bagguley, D., Ed.) pp 123–173, Oxford University Press, Oxford, U.K.

Evans, J. N. S., Appleyard, R. J., & Shuttleworth, W. A. (1992) *Bull. Magn. Reson. 14*, 81–85.

Evans, J. N. S., Appleyard, R. J., & Shuttleworth, W. A. (1993) *J. Am. Chem. Soc. 115*, 1588–1590.

Farber, G. K., Machin, P., Almo, S. C., Petsko, G. A., & Hajdu, J. (1988) *Proc. Natl. Acad. Sci. U.S.A. 85*, 112–115.

Fersht, A. (1985) in *Enzyme structure and function*, pp 193–195, W. H. Freeman, New York.

Fierke, L. A., Johnson, K. A., & Benkovic, S. J. (1987) *Biochemistry 26*, 4085–4092.

Frieden, C. (1993) *Trends Biochem. Sci. 18*, 58–60.

Garbow, J. R., & McWherter, A. (1993) *J. Am. Chem. Soc. 115*, 238–244.

Goldsack, D. E., Eberlein, S., & Alberty, R. A. (1965) *J. Biol. Chem. 240*, 4312–4315.

Gruys, K. J., Walker, M. C., & Sikorski, J. A. (1992) *Biochemistry 31*, 5534–5544.

Gruys, K. J., Marzabadi, M. R., Pansegrau, P. D., & Sikorski, J. A. (1993) *Arch. Biochem. Biophys. 304*, 345–351.

Gullion, T., & Schaefer, J. (1989) *J. Magn. Reson. 81*, 196–200.

Hajdu, J., & Johnson, L. N. (1990) *Biochemistry 29*, 1669–1678.

Hajdu, J., Acharya, K. R., Stuart, D. I., McLaughlin, P. J., Barford, D., Oikonomakos, N. G., Klein, H., & Johnson, L. N. (1987a) *EMBO J. 6*, 539–546.

Hajdu, J., Machin, P. A., Campbell, J. W., Greenhough, T. J., Clifton, I. J., Zurek, S., Glover, S., Johnson, L. N., & Elder, M. (1987b) *Nature 329*, 178–181.

Haw, J. F. (1988) *Anal. Chem. 60*, 559–570A.

Haw, J. F., Campbell, G. C., & Crosby, R. C. (1986) *Anal. Chem. 58*, 3172–3177.

Holl, S. M., McKay, R. A., Gullion, T., & Schaefer, J. (1990) *J. Magn. Reson. 89*, 620–626.

Lakshmi, K. V., Auger, M., Raap, J. J. L., Griffin, R. G., & Herzfeld, J. (1993) *J. Am. Chem. Soc. 115*, 8515–8516.

Leo, G. C., Sikorski, J. A., & Sammons, R. D. (1990) *J. Am. Chem. Soc. 112*, 1653–1654.

Levin, J. G., & Sprinson, D. B. (1964) *J. Biol. Chem. 239*, 1142–1150.

Lewendon, A., & Coggins, J. R. (1983) *Biochem. J. 213*, 187–191.

Marshall, G. R., Beusen, D. D., Kociolek, K. A., Redlinski, S., Leplawy, M. T., Pan, Y., & Schaefer, J. (1990) *J. Am. Chem. Soc. 112*, 963–966.

Martin, M. L., Delpuech, J.-J., & Martin, G. J. (1980) in *Practical NMR Spectroscopy*, pp 336–339, Heyden, London.

Mayer, E. (1985) *J. Appl. Phys. 58*, 663–667.

Moffat, K. (1989) *Annu. Rev. Biophys. Biophys. Chem. 18*, 309–332.

Padgette, S. R., Huyhn, Q. K., Bourgmeyer, J., Shah, D. M., Brand, L. A., Biest, R. D., Bishop, B. F., Rogers, S. G., Fraley, R. T., & Kishore, G. M. (1987) *Arch. Biochem. Biophys. 258*, 564–573.

Plattner, H., & Bachmann, L. (1982) *Int. Rev. Cytol. 79*, 237–304.

Raleigh, D. P., Levitt, M. H., & Griffin, R. G. (1988) *Chem. Phys. Lett. 146*, 71–76.

Ream, J. E., Yuen, H. K., Frazier, R. B., & Sikorski, J. A. (1992) *Biochemistry 31*, 5528–5534.

Sekhar, V. C., & Plapp, B. V. (1990) *Biochemistry 29*, 4289–4295.

Shuttleworth, W. A., Hough, C. D., Bertrand, K. P., & Evans, J. N. S. (1992) *Protein Eng. 5*, 461–466.

Van Geet, A. L. (1970) *Anal. Chem. 42*, 679–680.

Voelkel, R. (1988) *Angew. Chem., Int. Ed. Engl. 27*, 1468–1483.

Wehrle, B., Aguilar-Parrilla, F., & Limbach, H.-H. (1990) *J. Magn. Reson. 87*, 584–591.

Zimmerle, C. T., & Frieden, C. (1989) *Biochem. J. 258*, 381–387.

Zimmerle, C. T., Patane, K., & Freiden, C. (1987) *Biochemistry 26*, 6545–6552.